Carboxylic Acid Assisted Synthesis of Crystalline Silicon Derived from Coal Fly-Ash for Li-Ion Batteries Anode Material

Cornelius Satria Yudha
Chemical Engineering Department, UNS Vocational School, Universitas Sebelas Maret

Apriliyani, Enni
Chemical Engineering Department, UNS Vocational School, Universitas Sebelas Maret

Arinawati, Meidiana
Chemical Engineering Department, UNS Vocational School, Universitas Sebelas Maret

Paramitha, Tika
Centre of Excellence for Electrical Energy Storage Technology, Universitas Sebelas Maret

https://doi.org/10.5109/7236882

出版情報：Evergreen. 11 (3), pp.2395-2403, 2024-09. 九州大学グリーンテクノロジー研究教育センター
バージョン：

Carboxylic Acid Assisted Synthesis of Crystalline Silicon Derived from Coal Fly-Ash for Li-Ion Batteries Anode Material

Cornelius Satria Yudha[1,2,*], Enni Apriliyani[1,2], Meidiana Arinawati[1,2], Tika Paramitha[2]

[1]Chemical Engineering Department, UNS Vocational School, Universitas Sebelas Maret, Jl. Kol. Sutarto 150K Jebres, Surakarta 57126, Indonesia

[2]Centre of Excellence for Electrical Energy Storage Technology, Universitas Sebelas Maret, Surakarta 57146, Indonesia

*Author to whom correspondence should be addressed:
E-mail: corneliussyudha@staff.uns.ac.id

(Received October 29, 2023; Revised June 4, 2024; Accepted September 7, 2024).

Abstract: Demand for lithium-ion batteries (LIB) in wireless electronics, power tools, electric vehicles, and reliable energy storage systems is increasing. To meet lithium-ion battery (LIB) requirements, silicon or Si has been considered a state-of-the-art anode material owing to its significantly different specific capacity compared to the other anode. In this study, we attempted to synthesize crystalline Si (cSi) from coal combustion fly ash. The Si was prepared by caustic extraction, acidic precipitation, and magnesiothermic reduction of the as-obtained silica. Carboxylic acids, i.e. citric acid, acetic acid, and lactic acid, were used as the gelling agents. The SiO_2 and Si were characterized thoroughly to ensure the end-product quality. Based on our findings, the as-obtained SiO_2 samples are in an amorphous phase, while the as-obtained Si micro-powder has a highly crystalline structure. Based on the SEM-EDX analysis, the Si samples have high purity. In a full-cell LIB application, the pure Si anode coupled with $LiNi_{0.6}Co_{0.2}Mn_{0.2}O_2$ (NCM) cathode delivered poor electrochemical performance; however, when graphite was mechanically introduced Si, the performance was significantly improved. The Li-ion storage mechanism of Si/Graphite was investigated. The coal fly ash-derived Si powder can be utilized and modified to obtain Li-ion batteries with excellent electrochemical performance.

Keywords: Anode; Battery; Fly-ash; Material; Silicon, Waste

1. Introduction

Renewable energy sources have been widely researched because of the increasing environmental pollution and the rising number of energy needs as the number of people in the world grows. New and renewable energy generation largely depends on energy storage systems. Energy storage has been widely researched, especially in Lithium-Ion Batteries. The lithium-ion battery (LIB) was chosen because it is the most preferred power source for portable/wireless electronics, mobile applications, power tools, and energy storage systems. This is because LIBs have a distinctive high voltage quality, which results in considerable energy density and long cycle[1)]. The anode is an essential component in lithium-ion batteries. The anode that is used is graphite. Graphite was chosen because it is relatively cheap and easy to make electrodes. On the other hand, it has a considerably low of ~378 mAh/g (vs. Li/Li+), graphite was considered to be unable to meet the quality and increasing demands for high density, high safety, and long cycle-life energy storage; thus, new anode materials were developed[2–5)].

The silicon-based anode is expected to be the state-of-the-art anode active material for the next generation of high capacity and energy density LIBs owing to a theoretical capacity of ~4200 mAh/g. Unfortunately, using Si anode material has several drawbacks, such as low electrical conductivity. During the insertion and de-insertion of the Li-ion process, Si material experiences significant volume expansion (>300%). This expansion can cause material passivation, mainly from deformation and isolation from the main electrode phenomena. Another study proposed the utilization of reduced SiO_2 or silicon suboxide (SiOx) to elevate the structural stability of Si-based anode. In fact, SiO_x ($x < 2$) has a lower expected storage capacity of 1961 mAh/g than Si, but

SiO_x has less volume expansion, lower cost, and is environmentally friendly[6,7]. However, implementing SiO_x anode material also has disadvantages, such as relatively low conductivity and high irreversible coulombic efficiency during the initial cycle. Pre-lithiation of SiOx can be performed to improve the performance. However, cost-wise, this approach could be more beneficial[8].

To successfully apply Si as an anode material for the commercialization of high-capacity Li-ion batteries, the focus is not only on its performance-enhancing approach but also on the sustainability of the Si. Many efforts have been developed to obtain Si with excellent electrochemical performance. Still, they also often sacrifice the industrialization aspect, such as expensive and rare Si precursors complex, non-scalable, and energy-intensive processes[9,10]. By this technique, the Si material is no longer attractive for the sustainability of energy storage. Developing high-quality and high-purity Si material from cheap and abundant resources using a simple and facile production process is necessary, considering the economic and environmental aspects.

Due to today's reliability in coal-powered energy generation, coal-derived fly ash is continuously generated in large amounts. With the increasing energy demand, the coal exploitation rate has significantly increased. Aside from its carbon footprint, fly ash waste is also potentially harmful to living organisms and the environment. Due to the significant content of SiO_2, the fly ash can be utilized as the silica precursor during the production of silicon anode material[11,12].

In this report, high-purity silicon was produced from coal fly ash (CFA) obtained from the Indonesian Power Plant. Si is the dominant element in the CFA; however, further purification steps are required to obtain high-quality silicon powder: (i) caustic extraction of silica, (ii) organic acid-assisted precipitation, (iii) magnesiothermic reduction, and (iv) Si purification by acid leaching. The method does not use expensive chemicals and additives. The processing of CFA significantly improves its economic value and reduces its hazardous level. Carboxylic acids such as citric acid, acetic acid, and lactic acid are used as the gelling agent instead of mineral acids, further improving the safety and the eco-friendliness of the overall process[13,14]. The electrochemical performance of Si is investigated, especially in full Li-ion cells, which is rarely performed in research papers. The overall process can be considered highly efficient, scalable, cost-effective, and straightforward, and it can be directly applied to commercializing high-capacity LIBs.

2. Material and Methods

2.1. Materials

The CFA waste was obtained from the Paiton Power Plant, Probolinggo, Indonesia. NaOH flakes with 95% purity were obtained from PT Asahimas Chemical, Indonesia. Glacial acetic acid (Merck, Germany), 85% lactic acid (Merck, Germany), and citric acid monohydrate (Merck, Germany) were used as the gelling agent. Magnesium powder (Merck, Germany) was used as the reducing agent for SiO_2. All of these materials were used without any purification step.

2.2 Methodology

2.2.1 Preparation of Silica (SiO_2) Xerogel

SiO_2 content in CFA waste was extracted using a 4 M sodium hydroxide solution. The liquid per solid (L/S) ratio of coal extraction is 20 mL/g. The extraction process was performed in a 2 L beaker under vigorous stirring of 500 rpm at 60 ℃ for 4 hours. The resulting suspension was aged for 24 hours at room temperature. The residue from extraction was precipitated, and the supernatant was easily obtained via decantation. A demineralized water diluted the supernatant until the volume reached 2 L. This cloudy solution was labeled sodium meta-silicate solution and then separated into three 1-L beakers with identical volumes. 1 M of acetic acid (AA), lactic acid (LA), and citric acid (CA) were introduced to each respective beaker until the pH of the final solution was 7-8. During the reaction, the solutions were mixed at 300 rpm. After the desired pH is achieved, the white gel is formed. The pH was kept by adding acid dropwise for 1 hour. Next, the gel was aged for a day, filtered, and washed several times using deionized water and one time using ethanol to obtain the SiO_2 xerogels. The xerogels were vacuum-dried. The as-obtained SiO_2 were labeled according to the gelling agent, i.e., SiO_2-AA, SiO_2-LA, and SiO_2-CA.

2.2.2. Preparation of Silicon (Si) Powder

The as-prepared SiO_2 powders were ground and sieved using a 200-mesh screen. Each SiO_2 was mixed with magnesium (Mg) powder with a mass ratio of 4:5 or a molar ratio of 1:2. The solid-state mixing at lab-scale synthesis was performed using mortar and pestle until homogenous. In an alumina crucible, the mixture was fired in a box furnace at 750 ℃ for 2 hours under steady N_2 flow (PT. Samator Indonesia). After being cooled down, the as-obtained powders were dissolved in their respective acids with an L/S ratio of 50. During the leaching process, effervescence occurred. The leaching was stopped until the bubbles no longer appeared. The suspension was aged for 1 hour, and then the solids were separated using a paper filter. The solid was washed several times and vacuum dried at 90 ℃. The dried powder samples were ground and sieved using a 200-mesh screen and labeled according to the gelling and leaching agent, i.e., Si-AA, Si-LA, Si-CA, and Si-MA.

2.2.3. Material Characterization

To assure the quality of the SiO_2 and Si material, each sample characteristic was deeply investigated. FTIR spectroscope (IR-Spirit, Shimadzu, Japan) was used to analyze the surface functional group of the samples. The

structural properties and the purity of the samples were evaluated using XRD (MD10, Mini-diffractometer, MTI, USA). The morphological feature and element composition of the samples were investigated using a Scanning Electron Microscope- Energy Dispersive X-ray or SEM-EDX (JCM7000, Jeol, Japan). Further morphological characteristic analyses, such as surface area and pore dimension evaluation, were performed using the N_2 sorption isotherms technique at 77.35 K using a surface area analyzer (Quantachrome, USA). The thermogravimetric analysis was performed using a DTG-60 Thermogravimetric Analyzer (Shimadzu, Japan) under air atmosphere.

2.2.4. LiBs Cells Assembly and Testing

The silicon-based materials were applied as an anode material for Li-ion full batteries. Pure Si and 50% Si/G composite were separately coated on each side of a copper foil (MTI, USA). In the full-cell analysis, $LiNi_{0.6}Co_{0.2}Mn_{0.2}O_2$ or NCM was used as the counter cathode material. The electrode formulae and the controlled mass loading can be seen in Table 1. The overall assembly processes are similar to those of our previous study[11,15]. The fabricated cells were stored in a vacuum oven before the electrolyte filling (1M LiPF6 dissolved in ethylene carbonate-diethyl carbonate solvent). The cells were aged for a day before the electrochemical testing. The formation of the cells was performed using an Arbin Battery Analyzer (Arbin Instruments, USA) at a current density of 0.1 C (1C = 200 mA/gNCM) or 0.5 mA/cm^2 and a voltage window of 2.5-4.3 V. The cycle test was performed at 0.2 C for 50 times.

Table 1. Estimation of Cells Capacity

Type of electrodes	Formulae (active material: AB:CMC: SBR)	Mass Loading (mg/cm^2)	Theoretical Capacity	Estimated N/P
Pure Si-electrode	50:40:3:7	1.3-1.5	4200 mAh/g	1.05
50% Si/Graphite	70:20:3:7	2.8-3	2290 mAh/g	1.07
NCM	90:5:2:3	30-32	200 mAh/g	-

3. Result and Discussion

To obtain the silica from fly ash, it is necessary to investigate the characteristics of the CFA waste. Figure 1 (a) displays fly ash samples' TG/DTA curve. The CFA has a low mass loss of less than 0.2% as the temperature increases. This shows that the sample has a low loss of ignition value and low fixed carbon content. SEM image of the CFA depicted in Fig. 1(b) presents a micron-size particle with a near-perfect spherical shape. This phenomenon is consistent with previous studies, which also have reported a micron-sized spherical particle of coal-fly ash [16,17]. The composition of the coal-fly ash as EDX analysis results is listed in Table 2. Based on the result, Si, Al, Mg, Ca, and Fe have the highest composition based on weight or mol. The low content of Ca confirms that the fly ash is type F, which is effective for alkaline-based reactions or extraction[16,18].

Table 2. The EDX analysis result of coal-fly ash

Elements	Composition (wt%) (%)	Composition (mol%)
O	47.50	63.67
Mg	4.32	3.81
Al	12.90	10.25
Si	17.34	13.24
Ca	14.19	7.59
Fe	3.74	1.44
Sigma	100.00	100.00

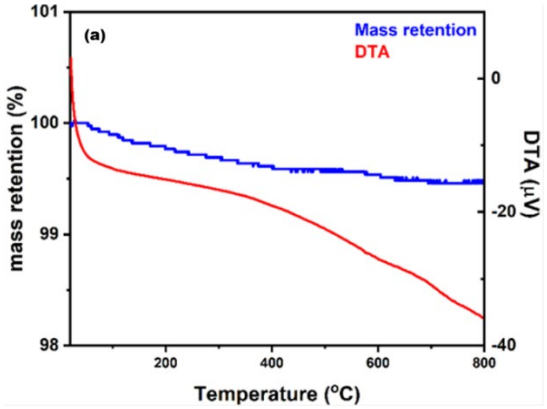

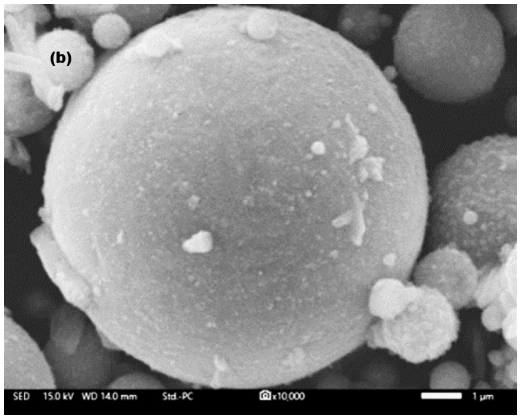

Fig. 1: (a) TG/DTA curve and (b) SEM Image of CFA

From XRD patterns presented in Fig. 2. a, SiO_2 AA, SiO_2-LA, and SiO_2-CA samples have a widening peak detected at a diffraction angle of 15–30◦; this explains that

three samples show an amorphous phase. In the three sample variations, no impurities were detected. In addition, all samples are appropriately indexed and are compliant with SiO_2 reference ICSD Card no. 061662[19,20]. These results prove that the variation in the use of different acid additions in the sample has no significant effect on the SiO_2 structure. FTIR spectra of SiO_2-AA, SiO_2-LA, and SiO_2-CA samples are shown in Fig. 2(b). As seen in the figure, the absorption at wavenumber 1110 cm^{-1}, 950 $cm^{-1,}$ and 790 cm^{-1} show Si-O-Si, Si-OH, and O-Si-O stretch vibration, respectively. Of all the types of vibrational bands formed from the sample, it is typically amorphous SiO_2[21,22]. Figure 2(c) presents the TG/DTA curve of the SiO_2 sample obtained using acetic acid, lactic acid, and citric acid. The TG curve confirms that there is a significant loss of mass of 13-15%. Based on the DTA analysis, the mass loss at less than 200 ℃ can be assigned to the endothermic evaporation of trapped water molecules in SiO_2 samples.]The following mass loss can be attributed to the exothermic decomposition of a residual organic compound, i.e., ethanol. Overall, the analysis confirmed that each SiO_2 sample has hydrophilicity, which attracts moisture from the atmosphere. To maintain the quality of SiO_2, the SiO_2 should be stored in a vacuum oven before the solid-state reduction reaction.

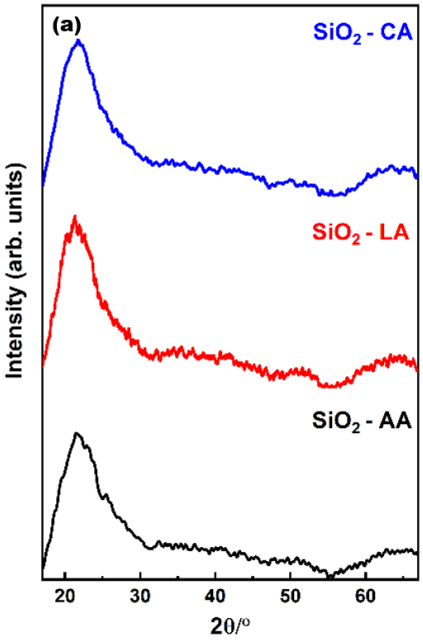

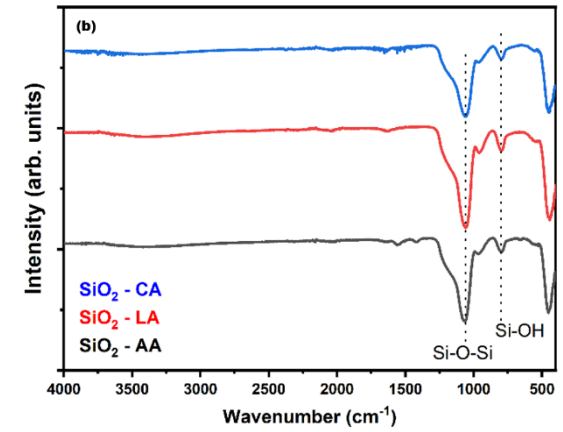

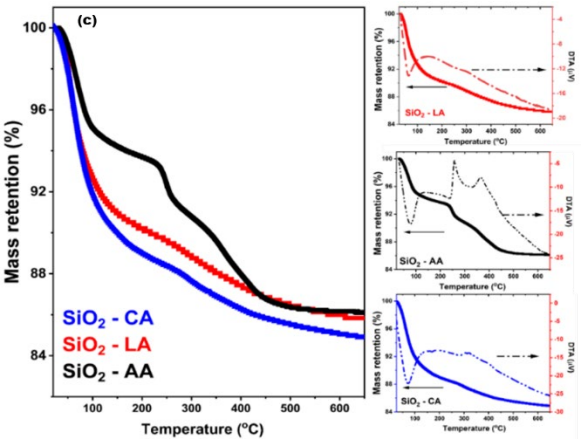

Fig. 2: (a) X-ray diffractogram, (b) FTIR-Spectra, and (c) TG/DTA of SiO_2 obtained using various acids

SEM Images of SiO_2 samples can be seen in Fig. 3. The images confirm the presence of micron-sized silica secondary particles that consist of submicron-sized primary particles. The formation of secondary particles might be affected by the Ostwald ripening effects. The primary particles formed through the densification of Si-OH nuclei, which increases as the reaction time is prolonged. The mapping of SiO_2 confirms the silicon dioxide component of the sample with no observable impurities. SiO_2 prepared using citric acid produces denser particles with smoother surfaces compared to the model prepared using acetic acid and lactic acid, in which the adherents of small particles are observed. Based on previous studies, gelation of SiO_2 by organic acids such as HCl, H_2SO_4, or HNO_3 often results in agglomerated submicron particles into polymorphs of secondary SiO_2. Unique-shaped SiO_2 particles such as spherical, nano-rods, nano-tubes, and nano-flowers are usually prepared using organo-silicon precursors such as tetra-ortho silicate (TEOS) or using advanced and complex procedures[12,23,24]. The formation of uniquely shaped SiO_2 from silica-containing waste is an interesting topic that will be developed in the future.

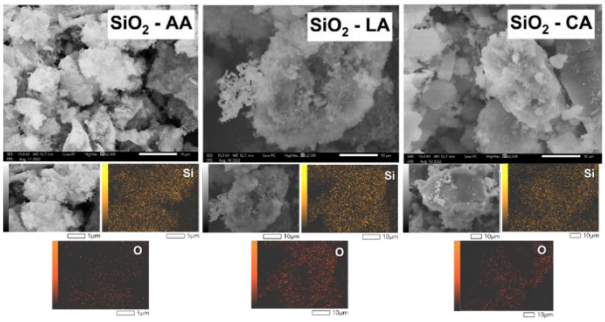

Fig. 3: SEM images and EDX Mappings of SiO_2 obtained using various acids: (a) acetic acid, (b) lactic acid, and (c) citric acid

Figure 4 shows an XRD analysis of silicon with various variations in acid addition. Silicon peaks formed on the curve are by the reference. Therefore, the magnesiothermic reduction of amorphous silica into crystalline silicon (cSi) is successfully conducted. In addition, silicon purification is also successful due to the dominant peaks of silicon in the diffractogram. However, there is a slight impurity phase assigned to magnesium silicate ($MgSiO_3$) in all of the samples, which is a side reaction during the magnesiothermic reduction. The crystalline silicon has a cubic diamond crystal structure with the dominant lattice point at the peak (111) at a diffraction angle of 28° of 2 theta formed in all three variations[25]. Overall, this shows that adding various types of acids also has no significant effect on the silicon structure. As seen in Fig. 4(b), the FT-IR spectrum of Si-CA, Si-LA, and Si-AA has formed peaks at wavenumber 860 cm^{-1} and 915 $cm^{-1,}$ which can be assigned to vibrations of silicon. In addition, the Si-O-Si stretching mode also found peaks at a wave number of 1070 $cm^{-1,}$ indicating oxygen's presence from an incomplete reduction process[26]. The oxygen appearance on the material's surface is considered usual since, in a previous study, there were additional washing steps using HF. Nevertheless, in this study, we decided to avoid harmful HF[14,27,28].

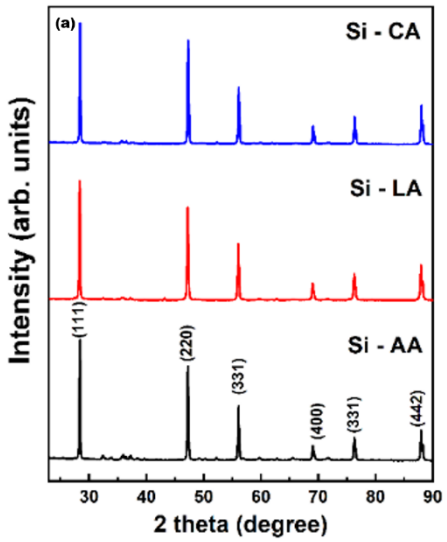

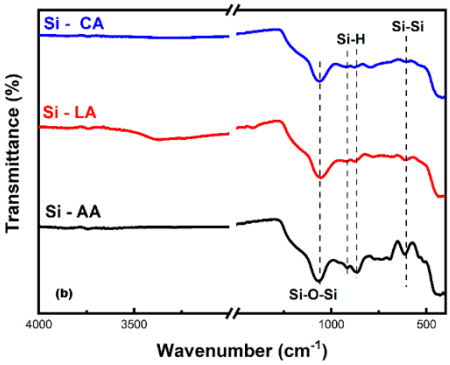

Fig. 4: (a) XRD of SiO_2 obtained using various acids: (a) acetic acid, (b) lactic acid, and (c) citric acid and (b) FTIR-Spectra of SiO_2 obtained using various acids: (a) acetic acid, (b) lactic acid, and (c) citric acid

Figure 5(a) displays the SEM-EDX analysis of the as-prepared silicon powders from the SiO_2 samples. Inhomogeneous-shaped micro-sized particles with rough surfaces can be observed for all silicon samples. The Si-AA and Si-LA prepared from SiO_2-AA and SiO_2-LA, respectively, have sub-micron-sized primary particles that can be seen. Meanwhile, the Si-CA sample has a denser and smoother morphology than the others. This proves that the magnesiothermic reduction process does not significantly alter the particle of SiO_2 precursor[29]. The presence of small oxygen in the EDX-Map of Si samples also proved that magnesium silicate exists on the surface of the particle. This was confirmed by the quantitative analysis using EDX, which is presented in Table 3. Si-AA exhibits high O and Mg content, which is consistent with the XRD result. The presence of magnesium silicate can be neglected. Based on these findings, the Si preparation can be summarized in the equations below:

$$SiO_2 + 2Mg \rightarrow Si \cdot MgO \quad (1)$$

$$Si \cdot MgO + 2HA \rightarrow \mathrm{Si} + \mathrm{MgA} + H_2O \quad (2)$$

Based on the reactions, the organic acid reacted with MgO and yielded soluble Mg-salt. We expect the reaction of AA with MgO to be slower due to the high pKa value of AA, causing the residual MgO in the sample. Meanwhile, LA and CA have higher pKa, which means stronger acidity compared with AA. Meanwhile, the pKa of CA is larger than the pKa of LA. Based on our data, the Mg content in Si-LA is lower. We predict that at the same concentration, the CA solution has higher viscosity due to the large molecular weight of CA. The viscous CA solution reduces the mass transfer during the reaction, which lowers the overall reaction kinetics.

The surface area analysis result shown in Fig. 5(b) is performed for LA samples. The surface area calculated using the BET method for SiO_2 - LA is 106.97 m^2/g with 8.5 nm, while after being converted into silicon powder, the surface area of Si – LA is reduced to 28.7 m^2/g with a pore diameter of 4.1 nm. Therefore, both SiO_2 - LA and Si – LA can be considered mesoporous with only a difference in the surface area value. This shows that during the magnesiothermic reduction, the particles

become denser, which is followed by a reduction in surface area. However, the densification also promotes pore shrinkage, which can be beneficial for energy storage applications. The adsorption and desorption of N_2 curves of SiO_2 and Si samples have type-IV shape curves, which confirm the presence of mesoporous materials[28,30].

Table 3. EDX Result of Si samples

Element	Si-AA (mol%)	Si-LA(mol%)	Si-CA(mol%)
Si	67.74	85.57	79.23
O	23.36	11.98	17.21
Mg	9.1	2.45	3.56

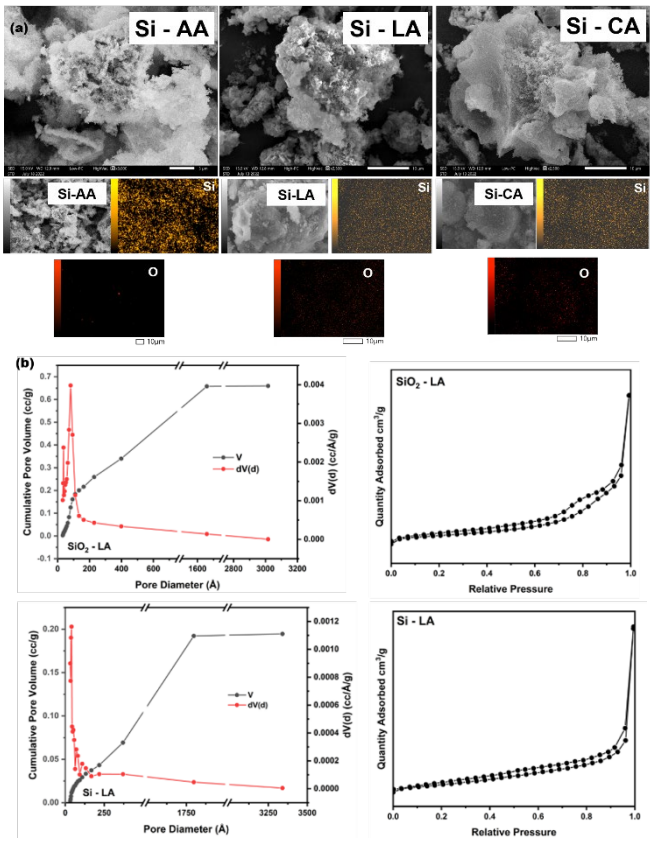

Fig. 5: (a) SEM images of SiO_2 obtained using various acids and (b) N_2 isotherm adsorption-desorption analysis of SiO_2 – LA and Si – LA

The charge-discharge analysis is conducted to evaluate the electrochemical performance of the as-prepared samples. Initially, we performed an analysis for pure samples. The charge-discharge and dQ/dV curves can be seen in Fig. 6(a) and (b), as we can see that the as-prepared Si material is able to operate similarly to commercial anodes such as graphite and other carbon-based materials. In theory, the commercial graphite has a lithiation and delithiation potential of 0.07-0.19 V and 0.1-0.23 V, respectively. Meanwhile, the lithiation and delithiation potential of Si is 0.05-0.21 and 0.31-0.47 V, respectively, almost similar to graphite. Therefore, the charge and discharge curve of Si-anode in LIBs full cell will be similar to a cell with graphite anode. When NCM622 is the cathode, the material is expected to operate at a voltage window of 2.5-4.3 V[31]. The charge capacity is 3.7 Ah/g, about ten times larger than graphite's. However, massive capacity loss occurs during discharge with a deliverable capacity of 1.17 Ah/g. The initial coulombic efficiency (ICE) of pure Si – LA is 31.6%, which is considered very poor. This phenomenon can be assigned to the electrochemical property of Si material, which often experiences expansion during the charging process. Based on the previous report, the expansion of Si material can achieve up to 270% from its initial volume[31,32]. The expansion can have a major effect on the battery system, such as pulverization of silicon during the shrinking process, which causes contact loss or isolation of material from the current collector or loss of electrical contact. This can cause significant capacity loss during cycling. Therefore, blending Si powder with commercial graphite can overcome this issue. The dQ/dV curve also confirms major phase alteration of NCM cathode material, which is also responsible for a capacity drop during the initial cycle[10,33].

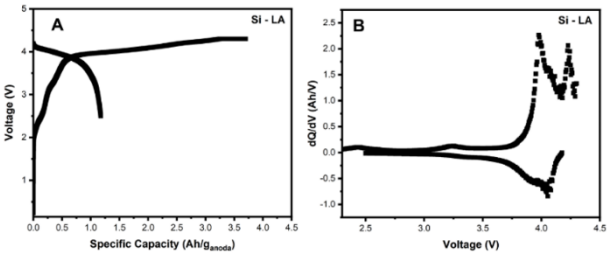

Fig. 6: Full Cells analysis of the as-prepared Si powders using Arbin Battery Analyzer: (A) Pure Si – LA charge-discharge analysis, (B) dQ/dV of pure Si – LA

To improve the ICE level of Si-based material, the as-prepared Si samples are composited with commercial graphite with a 50:50 composition. The composites were mixed using mortar and pestle for 30 minutes. The charge-discharge analysis is depicted in Fig. 7. The charge-discharge capacity of Si – AA, Si – LA, and Si - CA are 1.64 Ah/g /1.20 Ah/g, 1.71 Ah/g /1.22 Ah/g, and 1.67 Ah/g /1.15 Ah/g, respectively. Thus, the ICE of Si – AA, Si – LA, and Si – CA are 73.1%, 71.3%, and 69.2%, respectively. Si-LA achieves the highest discharge capacity; however, there are no significant differences between each sample. Based on the ICE, the discharge capacity and the dQ/dV value show significant improvements compared to the cell with pure Si powder as an anode. The effect of graphite in the composite is predicted to give better structural stability and compensate for the significant volume expansion of Si[34,35]. The dQ/dV vs. V curve confirms initial capacity loss due to the phase transformation of NCM cathode material[36–38].

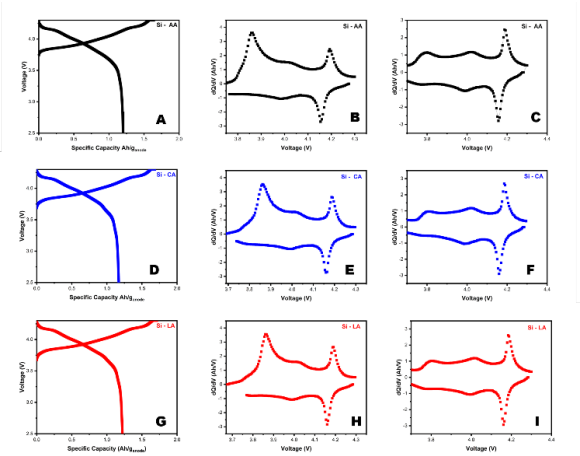

Fig. 7: Full Cells analysis using Arbin Battery Analyzer of (a-c) Si-AA/G, (d-f) Si-CA/G, and (g-h) Si-LA/G

The cycle performance of each cell is depicted in Fig. 8(a-c). The charge and discharge current were 0.2 C/ 0.2C (1C=200 mA/g). After 50 cycles, the capacity retention of Si-AA, Si-LA, and Si-CA are 20.11%, 24.92%, and 23.04% (Fig.8d), respectively. This means that the 50 w% Si is still large enough to be present as an anode, resulting in similar behavior to pure Si only at a prolonged cycle. However, the average coulombic efficiency is above 95%. The optimization of Si content in the composite is recommended to be investigated in future research.

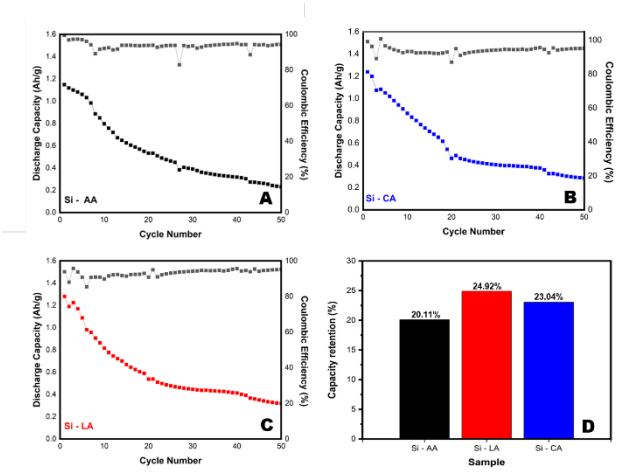

Fig. 8: Cycle Performance of (a) Si-AA/G, (b) Si-CA/G, and (c) Si-LA/G, and (d) Capacity Retention of Si-AA/G, Si-CA/G, and Si-LA/G

4. Conclusion

In this study, the synthesis of crystalline silicon (cSi) from alkaline extraction of silica followed by magnesiothermic reduction of F-type coal fly ash derived-silica is successfully performed. The extracted silica as the intermediate product has an amorphous structure and high purity, even derived from coal fly ash. Organic carboxylic acids successfully precipitate the silica xerogel, which improves the Eco-friendliness of the overall process. Based on the study, the carboxylic acids, i.e., acetic acid, lactic acid, and citric acid, do not significantly influence the structural properties of both SiO_2 and the final Si product. However, the particle morphology obtained using citric acid has the densest morphology and smooth surface. The EDX mapping of samples proved the dominance of the crystalline silicon (cSi) material. The as-prepared silicon powders were applied as the anode material of the NCM battery and could operate at a voltage range of 2.5-4.3 V based on the charge-discharge analysis with poor electrochemical performance. However, by compositing Si and commercial graphite (G), the cell achieved the highest discharge capacity of 1.22 Ah/$g_{Si\text{-}LA/G}$ with an initial coulombic efficiency of 71.3%. In the dQ/dV curve, a phase transformation of the NCM cathode can be detected as the reason for low coulombic efficiency. In the end, the study promises to be considered for the coal fly ash waste processing technique and polycrystalline silicon preparation.

Acknowledgments

We are thankful for the financial support from Universitas Sebelas Maret, Especially Lembaga Penelitian dan Pengabdian Masyarakat (LPPM through Fundamental Research (Penelitian Fundamental) scheme with contract no. 254/UN27.22/PT.01.03/2022 and228/UN27.22/PT.01.03/2023.

References

1) A.R. Nurohmah, C.S. Yudha, A. Purwanto, and H. Widiyandari, "Synthesis and characterization of nmc622 cathode material modified by various cheap and abundant transition metals for li-ion batteries synthesis and characterization of nmc622 cathode material modified by various cheap and abundant transition metals for," *Evergreen*, **9** (*2*) 427–437 (2022). https://doi.org/10.5109/4794168.
2) F. Holtstiege, A. Wilken, M. Winter, and T. Placke, "Running out of lithium? a route to differentiate between capacity losses and active lithium losses in lithium-ion batteries," *Physical Chemistry Chemical Physics*, **19** (*38*) 25905–25918 (2017). doi:10.1039/c7cp05405j.
3) B. Priyono, R. Baron, F. Zahara, and A. Subhan, "Enhancing performance of li4ti5o12 with addition of activated carbon from recycled pet waste as anode battery additives enhancing performance of li4ti5o12 with addition of activated carbon from recycled pet waste as anode battery additives," *Evergreen*, **9** (*2*) 563–570 (2022). https://doi.org/10.5109/4794188.
4) A.F. Ridassepri, F. Rahmawati, K.R. Heliani, Chairunnisa, J. Miyawaki, and A.T. Wijayanta, "Activated carbon from bagasse and its application for water vapor adsorption," *Evergreen*, **7** (*3*) 409–416 (2020). https://doi.org/10.5109/4068621.
5) C.S. Yudha, S.U. Muzayanha, H. Widiyandari, F. Iskandar, W. Sutopo, and A. Purwanto, "Synthesis of

lini0.85co0.14al0.01o2 cathode material and its performance in an nca / graphite full-battery," *Energies (Basel)*, **12** (*10*) (2019). doi:doi:10.3390/en12101886.

6) Z. Liu, Q. Yu, Y. Zhao, R. He, M. Xu, S. Feng, S. Li, L. Zhou, and L. Mai, "Silicon oxides: a promising family of anode materials for lithium-ion batteries," *Chem Soc Rev*, **48** (*1*) 285–309 (2019). doi:10.1039/c8cs00441b.
7) T. Chen, J. Wu, Q. Zhang, and X. Su, "Recent advancement of siox based anodes for lithium-ion batteries," *J Power Sources*, **363** 126–144 (2017). doi:10.1016/j.jpowsour.2017.07.073.
8) Y. Han, X. Liu, and Z. Lu, "Systematic investigation of prelithiated sio2 particles for high-performance anodes in lithium-ion battery," *Applied Sciences (Switzerland)*, **8** (*8*) (2018). doi:10.3390/app8081245.
9) R. Maddipatla, C. Loka, W.J. Choi, and K.S. Lee, "Nanocomposite of si/c anode material prepared by hybrid process of high-energy mechanical milling and carbonization for li-ion secondary batteries," *Applied Sciences (Switzerland)*, **8** (*11*) 1–12 (2018). doi:10.3390/app8112140.
10) H. Shi, X. Liu, R. Wu, Y. Zheng, Y. Li, X. Cheng, W. Pfleging, and Y. Zhang, "In situ sem observation of structured si/c anodes reactions in an ionic-liquid-based lithium-ion battery," *Applied Sciences (Switzerland)*, **9** (*5*) (2019). doi:10.3390/app9050956.
11) A. Jumari, C.S. Yudha, H. Widiyandari, and A.P. Lestari, "SiO2/c composite as a high capacity anode material of lini0.8co0.15al0.05o2 battery derived from coal combustion fly ash," *Applied Science*, **10** (*23*) 1–13 (2020). doi:https://doi.org/10.3390/app10238428.
12) X. Liu, Y. Chen, H. Liu, and Z.Q. Liu, "SiO2@C hollow sphere anodes for lithium-ion batteries," *J Mater Sci Technol*, **33** (*3*) 239–245 (2017). doi:10.1016/j.jmst.2016.07.021.
13) M.J. Campos-Molina, J.J. Corral-Pérez, R. Mariscal, and M.L. Granados, "Silica-poly(styrenesulphonic acid) nanocomposites as promising acid catalysts," *Catal Today*, **279** 155–163 (2017). doi:10.1016/j.cattod.2016.06.042.
14) X. Liu, Q. Zhang, Y. Zhu, J. Zhao, J. Chen, H. Ye, H. Wei, and Z. Liu, "Trash to treasure: harmful fly ash derived silicon nanoparticles for enhanced lithium-ion batteries," *Silicon*, **14** (*13*) 7983–7990 (2022). doi:10.1007/s12633-021-01528-z.
15) C.S. Yudha, A.P. Hutama, M. Rahmawati, and M. Arinawati, "Cathode material for high capacity nca / graphite secondary battery fabrication," 501–510 (2022).
16) D. Valeev, A. Mikhailova, and A. Atmadzhidi, "Kinetics of iron extraction from coal fly ash by hydrochloric acid leaching," *Metals (Basel)*, **8** (*7*) 1–9 (2018). doi:10.3390/met8070533.
17) P. Risdanareni, P. Puspitasari, and E. Januarti Jaya, "Chemical and physical characterization of fly ash as geopolymer material," *MATEC Web of Conferences*, **97** (2017). doi:10.1051/matecconf/20179701031.
18) A. Dindi, D.V. Quang, L.F. Vega, E. Nashef, and M.R.M. Abu-Zahra, "Applications of fly ash for co2 capture, utilization, and storage," *Journal of CO2 Utilization*, **29** (*November 2018*) 82–102 (2019). doi:10.1016/j.jcou.2018.11.011.
19) M.R. Babaa, A. Moldabayeva, M. Karim, A. Zhexembekova, Y. Zhang, Z. Bakenov, A. Molkenova, and I. Taniguchi, "Development of a novel sio2 based composite anode material for li-ion batteries," *Mater Today Proc*, **4** (*3*) 4542–4547 (2017). doi:10.1016/j.matpr.2017.04.027.
20) S. Affandi, H. Setyawan, S. Winardi, A. Purwanto, and R. Balgis, "A facile method for production of high-purity silica xerogels from bagasse ash," *Advanced Powder Technology*, **20** (*5*) 468–472 (2009). doi:10.1016/j.apt.2009.03.008.
21) H. Al Hijri, J.F. Fatriansyah, and N. Sofyan, "Potential use of corn cob waste as the base material of silica thin films for anti- reflective coatings potential use of corn cob waste as the base material of silica thin films for anti-reflective coatings," *Evergreen*, **9** (*1*) 102–108 (2022). https://doi.org/10.5109/4774221.
22) L.Y. Yu, Z.X. Huang, and M.X. Shi, "Synthesis and characterization of silica by sol-gel method," *Adv Mat Res*, **1030–1032** (*May 2017*) 189–192 (2014). doi:10.4028/www.scientific.net/AMR.1030-1032.189.
23) J.C. Echeverría, J. Estella, V. Barbería, J. Musgo, and J.J. Garrido, "Synthesis and characterization of ultramicroporous silica xerogels," *J Non Cryst Solids*, **356** (*6–8*) 378–382 (2010). doi:10.1016/j.jnoncrysol.2009.11.044.
24) T.G. Kim, G.S. An, J.S. Han, J.U. Hur, B.G. Park, and S.C. Choi, "Synthesis of size controlled spherical silica nanoparticles via sol-gel process within hydrophilic solvent," *Journal of the Korean Ceramic Society*, **54** (*1*) 49–54 (2017). doi:10.4191/kcers.2017.54.1.10.
25) J.O. Agunsoye, J.A. Adebisi, S.A. Bello, M. Haris, J.B. Agboola, and S.B. Hassan, "Synthesis of silicon nanoparticles from cassava periderm by reduction method," *Materials Science and Technology 2018, MS and T 2018*, (*January*) 701–709 (2019). doi:10.7449/2018/MST_2018_701_709.
26) T. Hülser, S.M. Schnurre, H. Wiggers, and C. Schulz, "Gas-phase synthesis of nanoscale silicon as an economical route towards sustainable energy technology," *KONA Powder and Particle Journal*, **29** (*February 2015*) 191–207 (2011). doi:10.14356/kona.2011021.
27) Z. Yan, J. Jiang, Y. Zhang, D. Yang, and N. Du, "Scalable and low-cost synthesis of porous silicon nanoparticles as high-performance lithium-ion battery anode," *Mater Today Nano*, **18** (*100175*) 1–9 (2022). doi:10.1016/j.mtnano.2022.100175.

28) N.S. Seroka, R.T. Taziwa, and L. Khotseng, "Extraction and synthesis of silicon nanoparticles (sinps) from sugarcane bagasse ash : a mini-review," *Applied Sciences (Switzerland)*, **12** (*2310*) 1–12 (2022). doi:app12052310.
29) I.H. Dwirekso, I.H. Dwirekso, and M. Ibadurrohman, "Synthesis of tio _ 2-sio _ 2-cuo nanocomposite material and its activities for self-cleaning synthesis of tio 2 -sio 2 -cuo nanocomposite material and its activities for self-cleaning," *Evergreen*, **7** (*2*) 285–291 (2020). https://doi.org/10.5109/4055234.
30) C. Anastasescu, S.P. Id, A. Rusu, D.C. Id, G.P. Id, S. Strungaru, J.M. Calderon-moreno, C.M. Id, C. Gifu, M. Enache, R. Socoteanu, D. Angelescu, and M. Anastasescu, "Tubular and spherical sio 2 obtained by sol gel method for lipase immobilization and enzymatic activity," *Molecules*, **23** (*1362*) 1–18 (2018). doi:10.3390/molecules23061362.
31) N. Nitta, F. Wu, J.T. Lee, and G. Yushin, "Li-ion battery materials: present and future," *Materials Today*, **18** (*5*) 252–264 (2015). doi:10.1016/j.mattod.2014.10.040.
32) Z. Xiao, C. Wang, L. Song, Y. Zheng, and T. Long, "Research progress of nano-silicon-based materials and silicon-carbon composite anode materials for lithium-ion batteries," *Journal of Solid State Electrochemistry*, **26** (*5*) 1125–1136 (2022). doi:10.1007/s10008-022-05141-x.
33) Y. Jiang, Y. Zhang, X. Yan, M. Tian, W. Xiao, and H. Tang, "A sustainable route from fly ash to silicon nanorods for high performance lithium ion batteries," *Chemical Engineering Journal*, **330** (*August*) 1052–1059 (2017). doi:10.1016/j.cej.2017.08.061.
34) J. Entwistle, A. Rennie, and S. Patwardhan, "A review of magnesiothermic reduction of silica to porous silicon for lithium-ion battery applications and beyond," *J Mater Chem A Mater*, **6** (*38*) 18344–18356 (2018). doi:10.1039/c8ta06370b.
35) S. He, S. Huang, S. Wang, I. Mizota, X. Liu, and X. Hou, "Considering critical factors of silicon/graphite anode materials for practical high-energy lithium-ion battery applications," *Energy and Fuels*, **35** (*2*) 944–964 (2021). doi:10.1021/acs.energyfuels.0c02948.
36) C.-H. Yim, S. Niketic, N. Salem, O. Naboka, and Y. Abu-Lebdeh, "Towards improving the practical energy density of li-ion batteries: optimization and evaluation of silicon:graphite composites in full cells," *J Electrochem Soc*, **164** (*1*) A6294–A6302 (2017). doi:10.1149/2.0481701jes.
37) C. Busà, M. Belekoukia, and M.J. Loveridge, "The effects of ambient storage conditions on the structural and electrochemical properties of nmc-811 cathodes for li-ion batteries," *Electrochim Acta*, **366** (2021). doi:10.1016/j.electacta.2020.137358.
38) C. Satria Yudha, E. Puspita Sari, D. Kurniawati Dewi, T. Paramitha, and W. Griyasti Suci, "Utilization of coal fly-ash derived silicon (si) as capacity enhancer of li-ion batteries anode material," *E3S Web of Conferences*, **481** 01007 (2024). doi:10.1051/e3sconf/202448101007.